Electronic Supplementary Material (ESI) for Journal of Materials Chemistry A.

Supporting Information

A membrane-less desalination battery with ultrahigh energy efficiency

Lu Guo[1], Yang Shang[1], Guangzhao Wang[2], Jun Jin[3], Zhi Yi Leong[1], Shaozhuan Huang[4], Chengding Gu[5], Meng Ding[1], Mei Er Pam[1], Sareh Vafakhah[1], Xueliang Li[1], Shengyuan A. Yang[2] and Hui Ying Yang *[1]

[1] Pillar of Engineering Product Development, Singapore University of Technology and Design, 8 Somapah Road, 487372, Singapore.

[2] Research Laboratory for Quantum Materials, Singapore University of Technology and Design, Singapore 487372, Singapore

[3] Faculty of Materials Science and Chemistry, China University of Geosciences, Wuhan, 430074, China

[4] Key Laboratory of Catalysis and Energy Materials Chemistry of Ministry of Education, South-Central University for Nationalities, Wuhan, Hubei, 430074, China

[5] School of materials and energy, Yunnan University, Kunming 650091, China

*Corresponding author. Tel.: +65 6303 6663; Fax: +65 6779 5161. E-mail address: yanghuiying@sutd.edu.sg (H. Y. Yang).

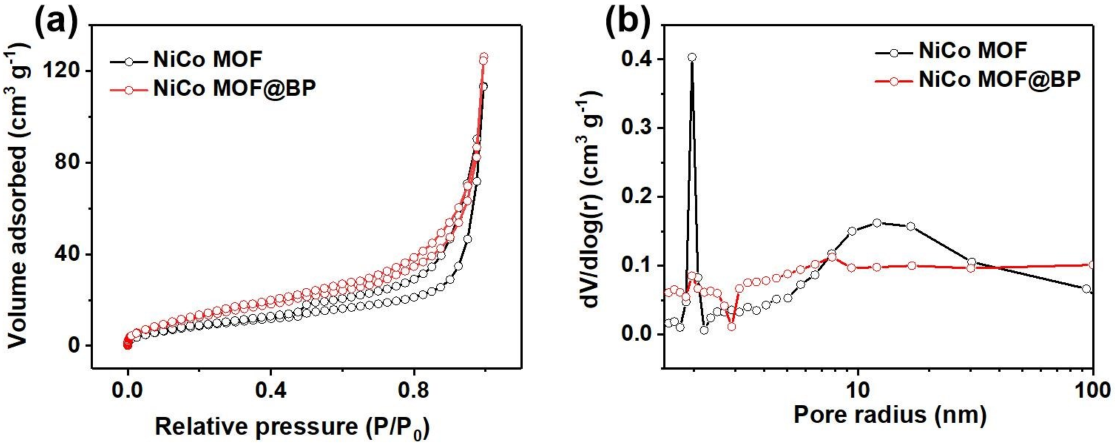

Figure S1. (a) Nitrogen sorption isotherms of NiCo MOF and NiCo MOF @BP. (b) BJH pore size distributions of NiCo MOF and NiCo MOF @BP.

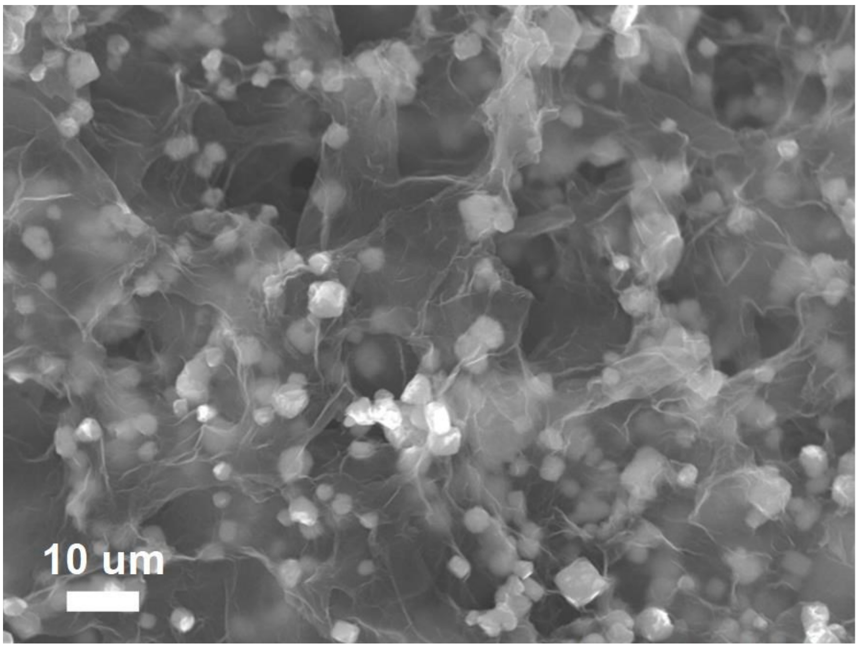

Figure S2. SEM image of the Ag@rGO anode.

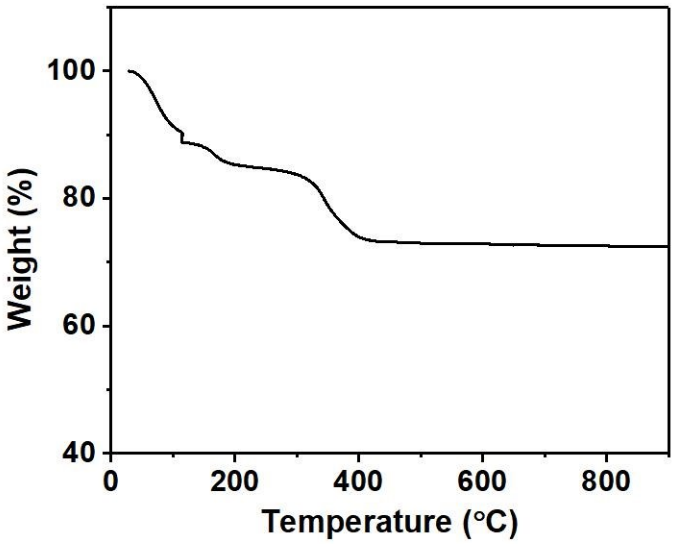

Figure S3. Thermogravimetric analysis (TGA) of Ag@rGO showing the weight loss in percent.

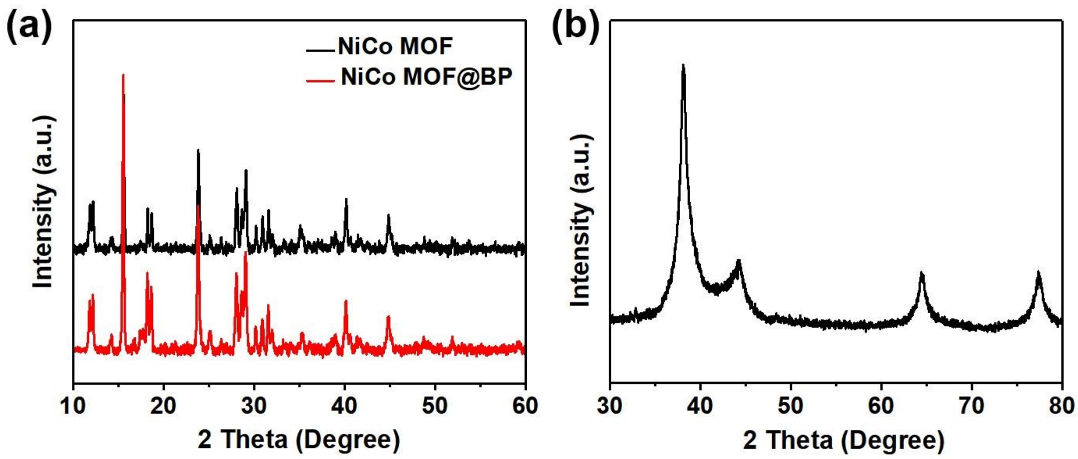

Figure S4. (a) Powder X-ray diffraction patterns of the as-prepared NiCo MOF, NiCo MOF @BP and (b) Ag@rGO.

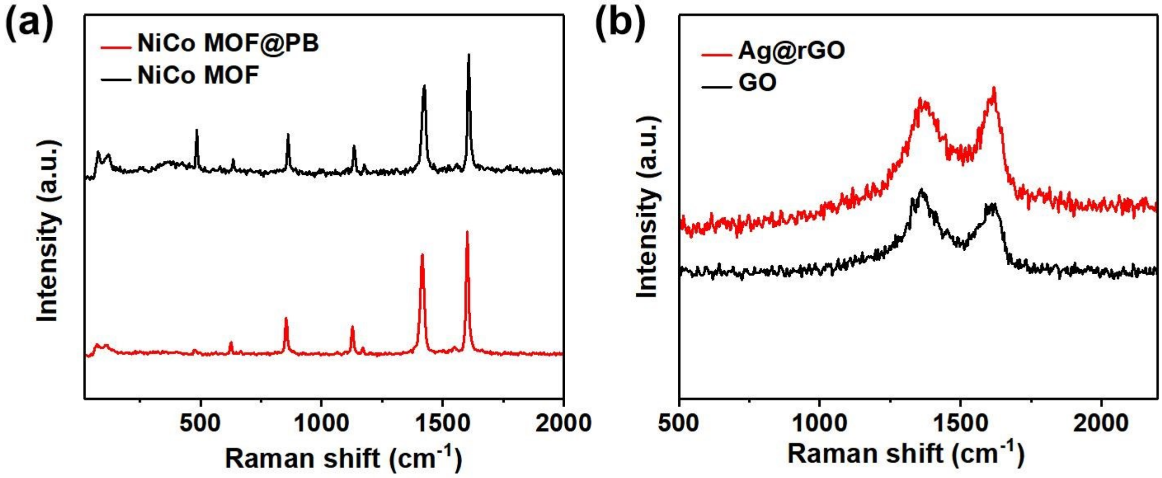

Figure S5. (a) Raman spectra of NiCo MOF and NiCo MOF @BP cathode. (b) Raman spectra of Ag@3DG and GO.

Characteristic A1g, B2g and A2g modes belonging to BP were observed for NiCo MOF@BP [1].

The Raman spectra of GO and Ag@rGO were studied. Typical peaks at 1350 cm^{-1} and 1580 cm^{-1} could be attributed to D and G bands of GO. After successful reduction, the value of I_D/I_G decreased from 1.01 to 0.99 which implied a higher degree of graphitization [2].

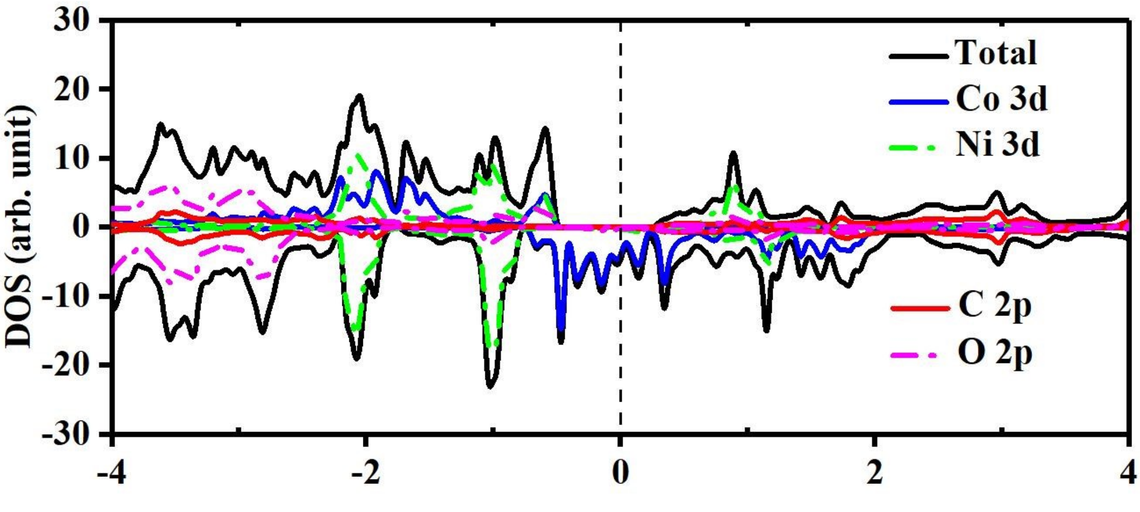

Figure S6. DOS of NiCo MOF. The Fermi level is set to 0.

Lattice parameters calculated for NiCo MOF were 20.06 Å × 3.29 Å × 6.22 Å, which agreed well with previous experimental values [3]. Spin up and down parts of the density of states (DOS) for NiCo MOF (Figure S6) were asymmetrical which suggested the existence of unpaired electrons. Based on these results, the total magnetic moment of NiCo MOF was calculated to be +6μB/ supercell where the main contributions from two Co (or Ni) atoms were +2.51/ +2.55 (or -1.50/ +1.59) μB/ supercell respectively. Additionally, an energy gap of 0.77 eV appeared in the spin up states whereas no energy gap was observed in the spin down states. The asymmetrical density of states illustrated the half-metallicity nature of NiCo MOF and the compromised electrical conductivity of NiCo MOF. As such, it was reasonable to incorporate a BP scaffold to enhance its electrical conductivity.

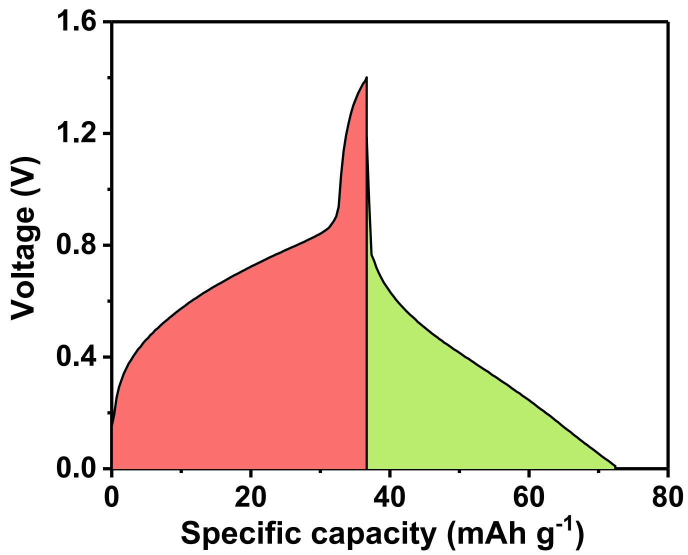

Figure S7. A typical galvanostatic charge/discharge curve of NiCo MOF@BP. Red region: charging process; green region: discharging process.

The chemical reaction equations of the two-stage sodium insertion/extraction process are indicated below:

$$Ni_xCo_{3-x}(OH)_2(C_8H_4O4)_2(H_2O)_4 + Na^+ + e^- \leftrightarrow NaNi_xCo_{3-x}\,O(OH)\,(C_8H_4O4)_2(H_2O)_4 \quad (1)$$

$$NaNi_xCo_{3-x}\,O(OH)\,(C_8H_4O4)_2(H_2O)_4 + Na^+ + e^- \leftrightarrow Na_2Ni_xCo_{3-x}\,O_2(C_8H_4O4)_2(H_2O)_4 \quad (2)$$

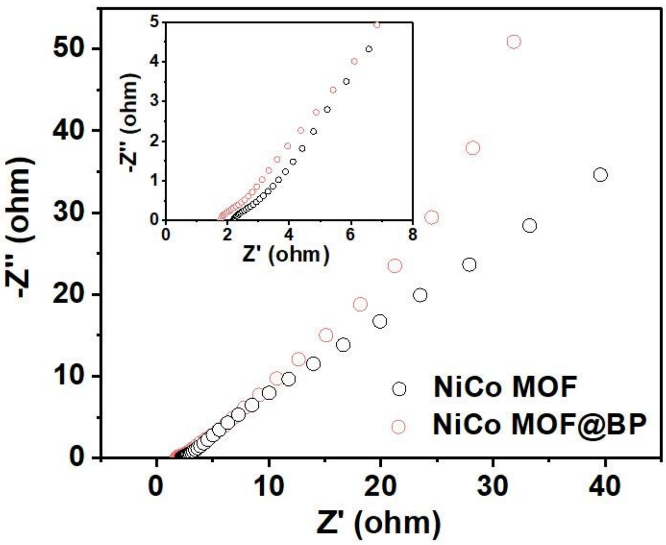

Figure S8. Nyquist spectra of NiCo MOF and NiCo MOF@BP after 20^{th} cycle.

Both cathodes show good electrical conductivity as indicated by their Nyquist plots. Understandably, the presence of BP in NiCo MOF@BP composite results in a slightly smaller interfacial resistance (R_s) and charge transfer resistance (R_{ct}).

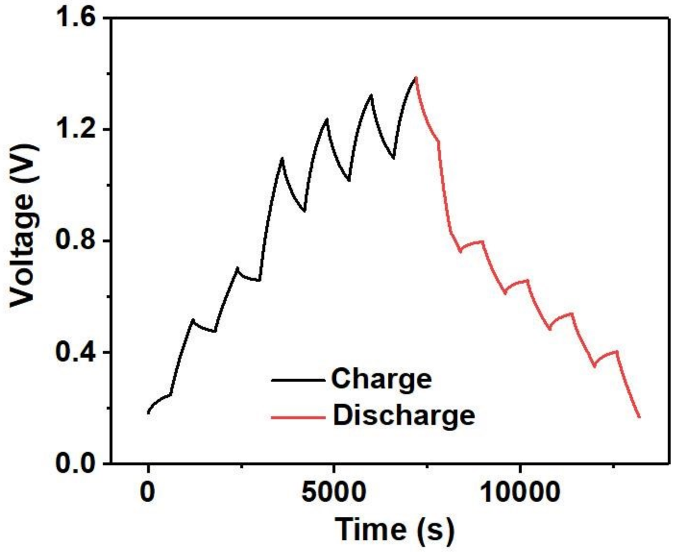

Figure S9. Galvanostatic intermittent titration technique (GITT) profiles of the NiCo MOF cathode in the desalination battery using a pulse current of 80 mA g^{-1} for 10min and intervals of 10 min in a stable cycle after 1-cycle activation process.

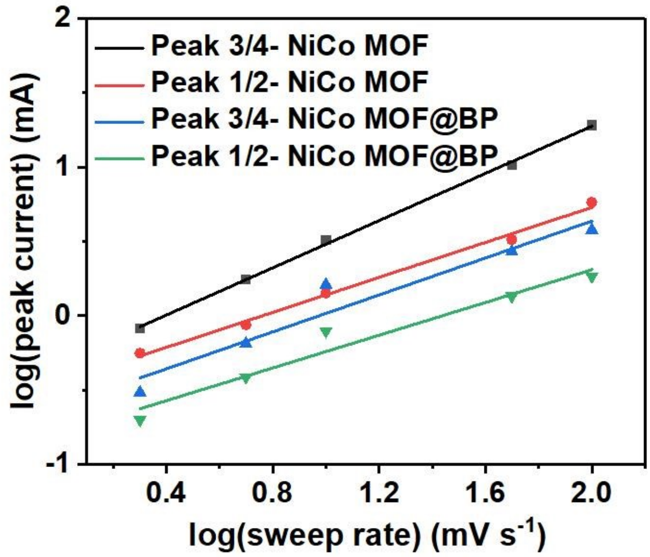

Figure S10. Log i-log v plots at two redox peaks of NiCo MOF and NiCo MOF @BP at various scan rates.

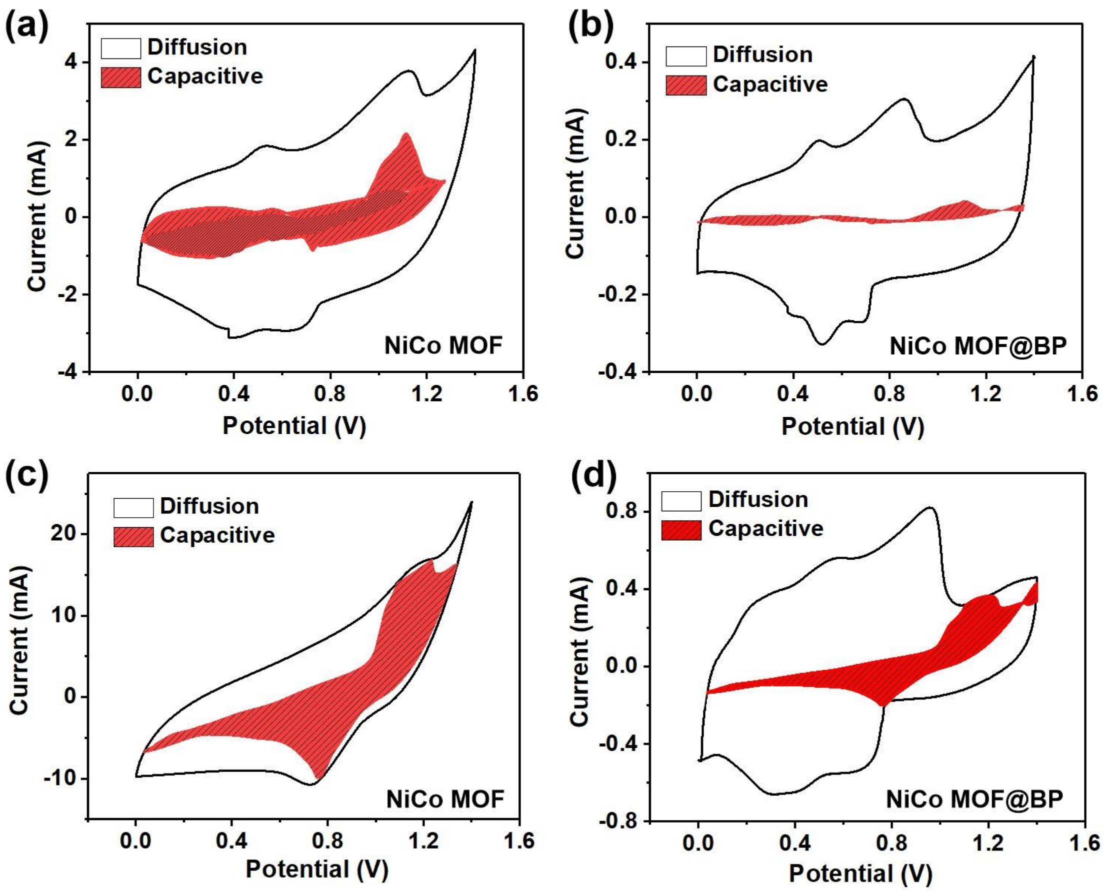

Figure S11. (a, b) CV curves indicate the surface capacitive contribution of NiCo MOF and NiCo MOF @BP at 2 and 100 mV s^{-1}.

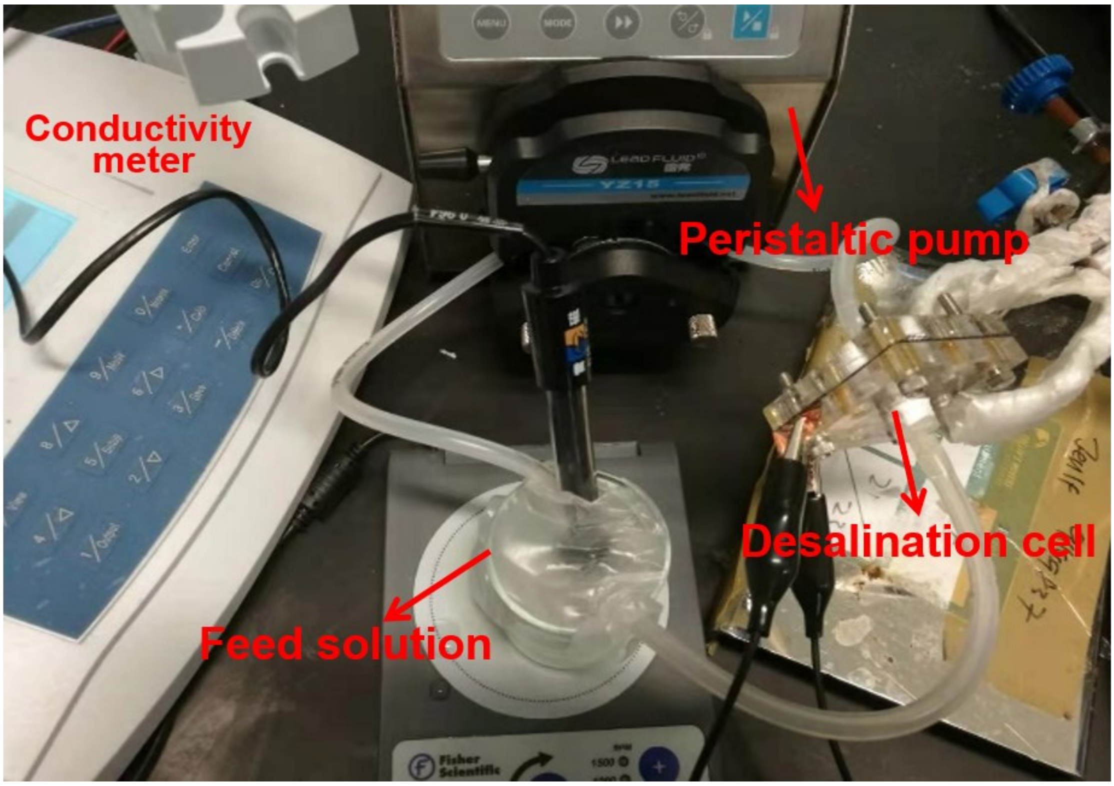

Figure S12. Photograph of the desalination cell configuration.

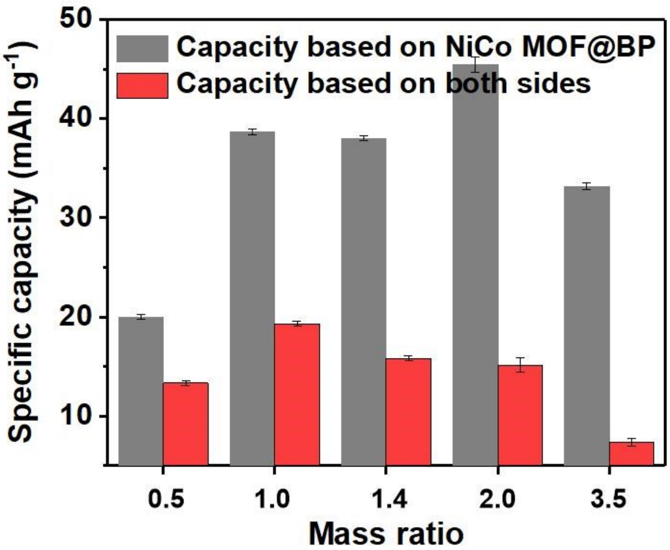

Figure S13. Specific capacity of the desalination battery with different mass ratio of Ag@rGO versus NiCo MOF@BP (red column: capacity calculated based on both side active materials; grey column: capacity calculated based on cathode side active material).

Table S1. The weight ratio of both electrodes

Weight / Weight ratio	Ag@rGO (mg)	NiCo MOF@BP (mg)
0.5	2	4
1.0	4	4
1.4	14	10
2.0	20	10
3.5	14	4

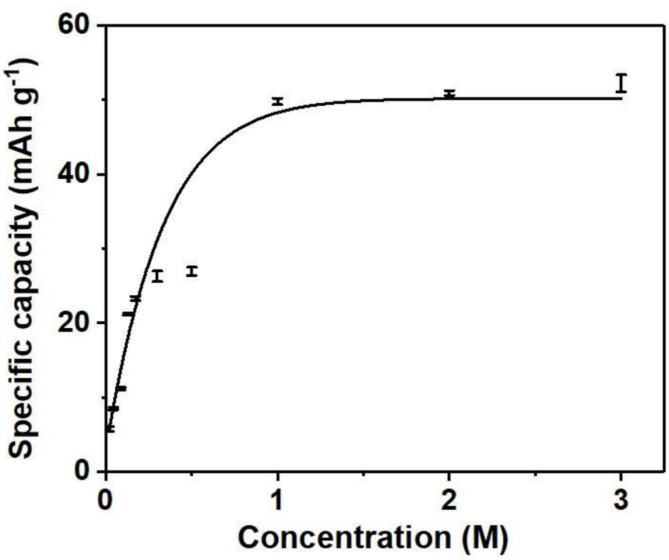

Figure S14. Specific capacity of the desalination battery with different feed concentration.

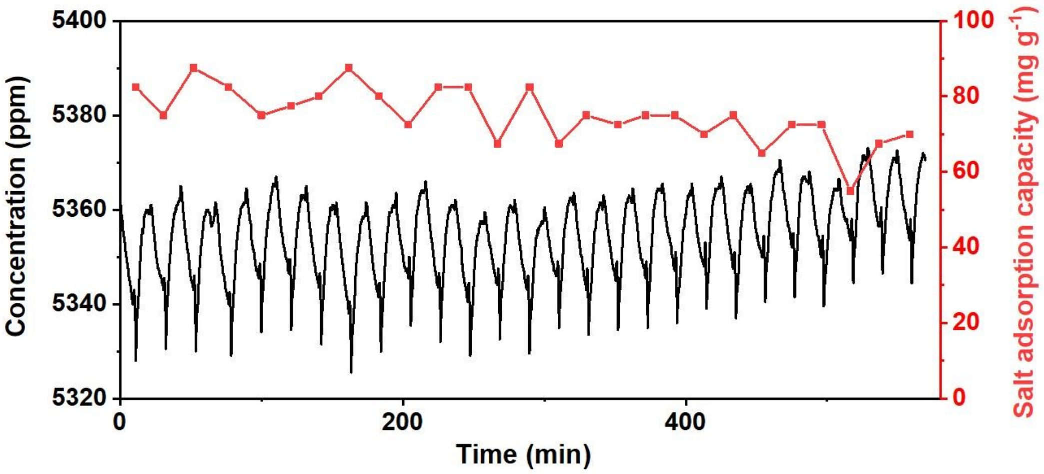

Figure S15. The concentration change profiles and the corresponding salt adsorption capacity for the desalination cycles.

To further explore the desalination performance of the full cell, this device is tested with a current density of 0.6 A g^{-1} and about 5000 ppm feed solution under real-time monitoring of the conductivity of the effluent. In a typical desalination cycle, the effluent concentration changes corresponding to the voltage variation. During the charging process, the sodium ions in influent migrate to the cathode materials, resulting in a conductivity decrease in the effluent, while chloride ions are removed by the Ag@rGO anode. The salt ions are released back into the electrolyte during the discharging process, causing the increase of the effluent concentration. As can be noticed, the effluent concentration varies inconsistently with the cell potential.

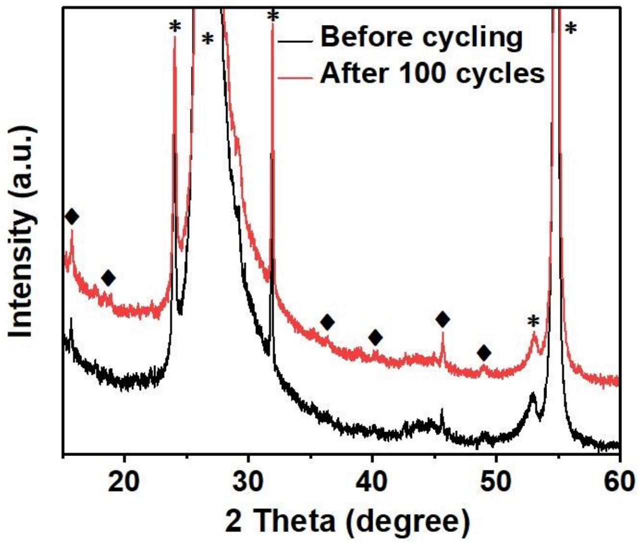

Figure S16. XRD patterns of NiCo MOF@BP electrode before and after long cycling in 2 M NaCl solution. The characteristic peaks for graphite paper substrate and NiCo MOF@BP nanosheets are marked by asterisk and diamond, respectively.

Table S1. Comparison of the desalination performance with different desalination system.

Electrode materials	Deionization system	Initial TDS (mg L^{-1})	Salt removal capacity (mg g^{-1})	Applied voltage (V)	Time (min)	Energy consumption (Wh g^{-1})	Energy recovery (%)	Publish year
Activated carbon	FCDI	35000	-	1.2	300	-	25	2019[4]
Nickel Hexacyanoferrate	CID	1170	34	1.5	54	0.035	-	2016[5]
Porous carbon	MCDI	1170	-	1.6	4	0.260	40	2012[6]
Porous carbon	cdi	1170	13	0.3-1.2	40	0.236	30	2015[7]
Porous carbon	MCDI	500	-	1.8	27	0.444	83	2013[8]

Activated carbon	CDI	468	13	1.2	20	0.342	-	2019[9]
Activated carbon	CDI	585	10.1	1.2	45	0.154	49.6	2019[10]
CuFe@NiFe PBA	MCDI	2925	71.8	1.0	240	0.0376	-	2019[11]
N, S-HTPC	CDI	500	25.95	1.2	150			2019[11]
Activated carbon	FCDI	5000	-	2.0	500	0.25	30	2019[12]
3D printed N-doped GO/CNT	MCDI	2500	75	1.4	100	0.331	27	2019[13]
Activated carbon	MCDI	2000	-	1.3	4	0.533	40	2020[14]
Ti_3C_2Tx MXene film	CDI	585	68	1.2	166	0.24	5.44	2020[15]
Ferricyanide	MC-RCDI	5850	67.8	1.2	2h	0.553		2019[16]
Carbon aerogel	CDI	5200	7.1	1.3	~120	0.21	30	2008[17]
NaI/VCl_2	FCDI	19000	-	0.3-1.1	~40	0.026	50	2018[18]
Ag coated porous carbon	MCDI	3900	23.2	0.7	20	0.348	-	2017[19]
CNT/graphene	CDI	780	26.42	2	~60	1.026		2013[20]
MOF derived porous carbon polyhedra	CDI	500	13.86	1.2	80			2015[21]
NMO	HCDI	5850	31.2	1.2	30			2014[22]

3D Graphene/Metal Oxide Nanoparticle Hybrids	CDI	6000	24.2	1.2	~3.8			2013[23]
Exfoliated MoS_2	CDI	23400	8.81	1.2	150			2017[24]
NiAl-LDH	CDI	585	81.2	1.2	~100			2014[25]
Sub-micrometer carbon beads	CDI	29250	11.5	1.2	60			2017[26]
$K_{0.03}Cu[Fe(CN)_6]_{0.65}\cdot 0.43H_2O$	CDI	500	23.2	1.2	100 (Half cycle)			2018[27]
N-doped 3D graphene	CDI	86	18.6	1.2	~14			2017[28]
N, P, S co-doped hollow carbon polyhedra	CDI	500	22.19	1.2	120 (Half cycle)			2018[29]
MnO_2	HCDI	500	14.9	1.0	10			2018[30]
MOF/polypyrrole hybrids	CDI	584	11.34	1.2	30 (Half cycle)			2019[31]
Manganese Oxide-Coated, Vertically Aligned CNTs	CDI	100	28.66	1.2	40 (Half cycle)			2018[32]
Hierarchical hole-	CDI	572	29.6	2	30 (Half			2018[3

enhanced 3D graphene					cycle)			[3]
3D intercalated graphene sheet–sphere nanocomposite	CDI	500	22.09	1.2	120 (Half cycle)			2018[34]
Tunnel structured manganese oxide nanowires	HCDI	1600	27.8	1.2	15 (Half cycle)			2018[35]
Porous Cryo-Dried MXene	CDI	10000	45	1.2	7.5 (Half cycle)			2018[36]
Iodide confined in Carbon Nanopores	FDI	5850	69	1	1 (Half cycle)	0.248		2018[37]
Activated carbon	HCDI	60g	-	1.2	-	0.44	36	2018[38]
$Na_{0.44}MnO_2$	MCDI	890	57.4	1.5	90			2017[39]
NMO	MCDI	760	68.5	1.5	120	0.46		2017[40]
Free-Standing Electrodes Derived from Metal–Organic Frameworks/ Nanofibers Hybrids	MCDI	1000	43.3	1.4	60			2018[41]

MOF-Derived TiO_2@Porous Carbon	MCDI	1500	46.7	1.4	60	0.319		2019[42]
Bimetallic MOF derived porous carbon	MCDI	750	45.62	1.4	120			2017[2]
$FePO_4$/RGO	MCDI	750	100	1.4	210	0.357	35	2018[36]
$Li_4Ti_5O_{12}$@C	MCDI	2500	25	1.4	120	0.284		2019[43]
Prussian blue	MCDI	700	96	1.4	30	0.079	40	2017[44]
Ar plasma modification of 2D MXene $Ti_3C_2T_x$	CDI	500	26.8	1.4	30			2018[45]
$NaTi_2(PO_4)_3$/rGO	MCDI	1000	120	1.4	60			2017[46]
$NaTi_2(PO_4)_3$-AgNPs	MCDI	2500	105	1.4	70	0.127	30	2018[47]
3D graphene oxide and polyvinyl alcohol composites	CDI	250	36.1	1.2	60			2017[48]
Freestanding PB/Graphene Aerogel	MCDI	2500	130	1.4	130	0.23	39	2019[49]
$Na_3V_2(PO_4)_3$@C	MCDI	1000	98	1.4	120			2018[50]
$Na_3V_2(PO_4)_3$/graphene aerogel	MCDI	1000	107.5	1.4	105			2019[51]

NiCo MOF@P	CDI	1M	103.1	1.4	20	0.034	67.01	This work

Reference:

1. A. Favron, F. A. Goudreault, V. Gosselin, J. Groulx, M. Cote, R. Leonelli, J. F. Germain, A. L. Phaneuf-L'Heureux, S. Francoeur and R. Martel, *Second-Order Raman Scattering in Exfoliated Black Phosphorus*, *Nano letters*, 2018, **18**, 1018-1027.
2. M. Ding, W. Shi, L. Guo, Z. Y. Leong, A. Baji and H. Y. Yang, *Bimetallic metal–organic framework derived porous carbon nanostructures for high performance membrane capacitive desalination*, *J. Mater. Chem. A*, 2017, **5**, 6113-6121.
3. S. Zhao, Y. Wang, J. Dong, C.-T. He, H. Yin, P. An, K. Zhao, X. Zhang, C. Gao, L. Zhang, J. Lv, J. Wang, J. Zhang, A. M. Khattak, N. A. Khan, Z. Wei, J. Zhang, S. Liu, H. Zhao and Z. Tang, *Ultrathin metal–organic framework nanosheets for electrocatalytic oxygen evolution*, *Nature Energy*, 2016, **1**.
4. H. Lim, Y. Ha, H. B. Jung, P. S. Jo, H. Yoon, D. Quyen, N. Cho, C.-Y. Yoo and Y. Cho, *Energy storage and generation through desalination using flow-electrodes capacitive deionization*, *Journal of Industrial and Engineering Chemistry*, 2020, **81**, 317-322.
5. S. Porada, P. Bukowska, A. Shrivastava, P. Biesheuvel and K. C. Smith, *Nickel Hexacyanoferrate Electrodes for Cation Intercalation Desalination*, *arXiv preprint arXiv:1612.08293*, 2016.
6. R. Zhao, P. M. Biesheuvel and A. van der Wal, *Energy consumption and constant current operation in membrane capacitive deionization*, *Energy & Environmental Science*, 2012, **5**, 9520.
7. T. Kim, J. E. Dykstra, S. Porada, A. van der Wal, J. Yoon and P. M. Biesheuvel, *Enhanced charge efficiency and reduced energy use in capacitive deionization by increasing the discharge voltage*, *Journal of colloid and interface science*, 2015, **446**, 317-326.
8. P. Dlugolecki and A. van der Wal, *Energy recovery in membrane capacitive deionization*, *Environmental science & technology*, 2013, **47**, 4904-4910.
9. Y.-J. Chen, C.-F. Liu, C.-C. Hsu and C.-C. Hu, *An integrated strategy for improving the desalination performances of activated carbon-based capacitive deionization systems*, *Electrochimica Acta*, 2019, **302**, 277-285.
10. Y.-W. Chen, J.-F. Chen, C.-H. Lin and C.-H. Hou, *Integrating a supercapacitor with capacitive deionization for direct energy recovery from the desalination of brackish water*, *Applied Energy*, 2019, **252**, 113417.
11. Y. Zhao, B. Liang, X. Wei, K. Li, C. Lv and Y. Zhao, *A core–shell heterostructured CuFe@NiFe Prussian blue analogue as a novel electrode material for high-capacity and stable capacitive deionization*, *Journal of Materials Chemistry A*, 2019, **7**, 10464-10474.
12. C. Zhang, L. Wu, J. Ma, A. N. Pham, M. Wang and T. D. Waite, *Integrated Flow-Electrode Capacitive Deionization and Microfiltration System for Continuous and Energy-Efficient Brackish Water Desalination*, *Environmental science & technology*, 2019, **53**, 13364-13373.
13. S. Vafakhah, G. J. Sim, M. Saeedikhani, X. Li, P. Valdivia y Alvarado and H. Y. Yang, *3D*

printed electrodes for efficient membrane capacitive deionization, *Nanoscale Advances*, 2019, **1**, 4804-4811.

14. C. Tan, C. He, J. Fletcher and T. D. Waite, *Energy recovery in pilot scale membrane CDI treatment of brackish waters*, *Water research*, 2020, **168**, 115146.
15. J. Ma, Y. Cheng, L. Wang, X. Dai and F. Yu, *Free-standing $Ti_3C_2T_x$ MXene film as binder-free electrode in capacitive deionization with an ultrahigh desalination capacity*, *Chemical Engineering Journal*, 2020, **384**, 123329.
16. N. Kim, S. P. Hong, J. Lee, C. Kim and J. Yoon, *High-Desalination Performance via Redox Couple Reaction in the Multichannel Capacitive Deionization System*, *ACS Sustainable Chemistry & Engineering*, 2019, **7**, 16182-16189.
17. P. Xu, J. E. Drewes, D. Heil and G. Wang, *Treatment of brackish produced water using carbon aerogel-based capacitive deionization technology*, *Water research*, 2008, **42**, 2605-2617.
18. F. Chen, X. Hou, Q. Liang, X. Hu, Y. Zhou, Q. Ru and S.-J. Hu, *Coupling Desalination and Energy Storage with Redox Flow Electrodes*, *Nanoscale*, 2018, DOI: 10.1039/c8nr02737d.
19. H. Yoon, J. Lee, S. Kim and J. Yoon, *Hybrid capacitive deionization with Ag coated carbon composite electrode*, *Desalination*, 2017, **422**, 42-48.
20. Y. Wimalasiri and L. Zou, *Carbon nanotube/graphene composite for enhanced capacitive deionization performance*, *Carbon*, 2013, **59**, 464-471.
21. Y. Liu, X. Xu, M. Wang, T. Lu, Z. Sun and L. Pan, *Metal–organic framework-derived porous carbon polyhedra for highly efficient capacitive deionization*, *Chemical communications*, 2015, **51**, 12020-12023.
22. J. Lee, S. Kim, C. Kim and J. Yoon, *Hybrid capacitive deionization to enhance the desalination performance of capacitive techniques*, *Energy Environ. Sci.*, 2014, **7**, 3683-3689.
23. H. Yin, S. Zhao, J. Wan, H. Tang, L. Chang, L. He, H. Zhao, Y. Gao and Z. Tang, *Three-dimensional graphene/metal oxide nanoparticle hybrids for high-performance capacitive deionization of saline water*, *Advanced materials*, 2013, **25**, 6270-6276.
24. F. Xing, T. Li, J. Li, H. Zhu, N. Wang and X. Cao, *Chemically exfoliated MoS_2 for capacitive deionization of saline water*, *Nano Energy*, 2017, **31**, 590-595.
25. X. Lei, B. Wang, J. Liu, Z. Ye, Z. Chang, M. Jiang and X. Sun, *Three-dimensional NiAl-mixed metal oxide film: preparation and capacitive deionization performances*, *RSC Adv.*, 2014, **4**, 41642-41648.
26. B. Krüner, P. Srimuk, S. Fleischmann, M. Zeiger, A. Schreiber, M. Aslan, A. Quade and V. Presser, *Hydrogen-treated, sub-micrometer carbon beads for fast capacitive deionization with high performance stability*, *Carbon*, 2017, **117**, 46-54.
27. S. Choi, B. Chang, S. Kim, J. Lee, J. Yoon and J. W. Choi, *Battery Electrode Materials with Omnivalent Cation Storage for Fast and Charge-Efficient Ion Removal of Asymmetric Capacitive Deionization*, *Advanced Functional Materials*, 2018, DOI: 10.1002/adfm.201802665, 1802665.
28. A. M. Abdelkader and D. J. Fray, *Controlled electrochemical doping of graphene-based 3D nanoarchitecture electrodes for supercapacitors and capacitive deionisation*, *Nanoscale*, 2017, **9**, 14548-14557.
29. J. Zhang, J. Fang, J. Han, T. Yan, L. Shi and D. Zhang, *N, P, S co-doped hollow carbon polyhedra derived from MOF-based core–shell nanocomposites for capacitive deionization*,

Journal of Materials Chemistry A, 2018, **6**, 15245-15252.

30. T. Wu, G. Wang, S. Wang, F. Zhan, Y. Fu, H. Qiao and J. Qiu, *Highly Stable Hybrid Capacitive Deionization with a MnO_2 Anode and a Positively Charged Cathode*, *Environmental Science & Technology Letters*, 2018, **5**, 98-102.
31. Z. Wang, X. Xu, J. Kim, V. Malgras, R. Mo, C. Li, Y. Lin, H. Tan, J. Tang, L. Pan, Y. Bando, T. Yang and Y. Yamauchi, *Nanoarchitectured metal–organic framework/polypyrrole hybrids for brackish water desalination using capacitive deionization*, *Materials Horizons*, 2019, **6**, 1433-1437.
32. W. Shi, X. Zhou, J. Li, E. R. Meshot, A. D. Taylor, S. Hu, J.-H. Kim, M. Elimelech and D. L. Plata, *High-Performance Capacitive Deionization via Manganese Oxide-Coated, Vertically Aligned Carbon Nanotubes*, *Environmental Science & Technology Letters*, 2018, **5**, 692-700.
33. J. Li, B. Ji, R. Jiang, P. Zhang, N. Chen, G. Zhang and L. Qu, *Hierarchical hole-enhanced 3D graphene assembly for highly efficient capacitive deionization*, *Carbon*, 2018, **129**, 95-103.
34. Z. U. Khan, T. Yan, L. Shi and D. Zhang, *Improved capacitive deionization by using 3D intercalated graphene sheet–sphere nanocomposite architectures*, *Environmental Science: Nano*, 2018, **5**, 980-991.
35. B. W. Byles, D. A. Cullen, K. L. More and E. Pomerantseva, *Tunnel structured manganese oxide nanowires as redox active electrodes for hybrid capacitive deionization*, *Nano Energy*, 2018, **44**, 476-488.
36. W. Bao, X. Tang, X. Guo, S. Choi, C. Wang, Y. Gogotsi and G. Wang, *Porous Cryo-Dried MXene for Efficient Capacitive Deionization*, *Joule*, 2018, **2**, 778-787.
37. J. Lee, P. Srimuk, S. Carpier, J. Choi, R. L. Zornitta, C. Kim, M. Aslan and V. Presser, *Confined Redox Reactions of Iodide in Carbon Nanopores for Fast and Energy-Efficient Desalination of Brackish Water and Seawater*, *ChemSusChem*, 2018, **11**, 3460-3472.
38. A. Rommerskirchen, C. J. Linnartz, D. Müller, L. K. Willenberg and M. Wessling, *Energy Recovery and Process Design in Continuous Flow–Electrode Capacitive Deionization Processes*, *ACS Sustainable Chemistry & Engineering*, 2018, **6**, 13007-13015.
39. F. Chen, Y. Huang, L. Guo, M. Ding and H. Y. Yang, *A dual-ion electrochemistry deionization system based on AgCl-NMO Electrodes*, *Nanoscale*, 2017, DOI: 10.1039/c7nr01861d.
40. F. Chen, Y. Huang, L. Guo, L. Sun, Y. Wang and H. Y. Yang, *Dual-ions electrochemical deionization: a desalination generator*, *Energy Environ. Sci.*, 2017, DOI: 10.1039/c7ee00855d.
41. M. Ding, K. K. R. Bannuru, Y. Wang, L. Guo, A. Baji and H. Y. Yang, *Free-Standing Electrodes Derived from Metal-Organic Frameworks/ Nanofibers Hybrids for Membrane Capacitive Deionization*, *Advanced Materials Technologies*, 2018, **3**, 1800135.
42. M. Ding, S. Fan, S. Huang, M. E. Pam, L. Guo, Y. Shi and H. Y. Yang, *Tunable Pseudocapacitive Behavior in Metal–Organic Framework-Derived TiO_2@Porous Carbon Enabling High-Performance Membrane Capacitive Deionization*, *ACS Applied Energy Materials*, 2019, **2**, 1812-1822.
43. L. Guo, D. Kong, M. E. Pam, S. Huang, M. Ding, Y. Shang, C. Gu, Y. Huang and H. Y. Yang, *The efficient faradaic $Li_4Ti_5O_{12}$@C electrode exceeds the membrane capacitive desalination performance*, *Journal of Materials Chemistry A*, 2019, **7**, 8912-8921.
44. L. Guo, R. Mo, W. Shi, Y. Huang, Z. Y. Leong, M. Ding, F. Chen and H. Y. Yang, *A*

Prussian blue anode for high performance electrochemical deionization promoted by the faradaic mechanism, *Nanoscale*, 2017, DOI: 10.1039/c7nr03579a.

45. L. Guo, X. Wang, Z. Y. Leong, R. Mo, L. Sun and H. Y. Yang, *Ar plasma modification of 2D MXene $Ti_3C_2T_x$ nanosheets for efficient capacitive desalination*, *FlatChem*, 2018, **8**, 17-24.
46. Y. Huang, F. Chen, L. Guo and H. Y. Yang, *Ultrahigh performance of a novel electrochemical deionization system based on a $NaTi_2(PO_4)_3$/rGO nanocomposite*, *J. Mater. Chem. A*, 2017, DOI: 10.1039/c7ta03725b.
47. Y. Huang, F. Chen, L. Guo, J. Zhang, T. Chen and H. Y. Yang, *Low energy consumption dual-ion electrochemical deionization system using $NaTi_2(PO_4)_3$-AgNPs electrodes*, *Desalination*, 2018, DOI: 10.1016/j.desal.2018.02.006.
48. Z. Y. Leong, G. Lu and H. Y. Yang, *Three-dimensional graphene oxide and polyvinyl alcohol composites as structured activated carbons for capacitive desalination*, *Desalination*, 2017, DOI: 10.1016/j.desal.2017.07.018.
49. S. Vafakhah, L. Guo, D. Sriramulu, S. Huang, M. Saeedikhani and H. Y. Yang, *Efficient Sodium-Ion Intercalation into the Freestanding Prussian Blue/Graphene Aerogel Anode in a Hybrid Capacitive Deionization System*, *ACS applied materials & interfaces*, 2019, **11**, 5989-5998.
50. W. Zhao, L. Guo, M. Ding, Y. Huang and H. Y. Yang, *Ultrahigh-Desalination-Capacity Dual-Ion Electrochemical Deionization Device Based on $Na_3V_2(PO_4)_3$@C-AgCl Electrodes*, *ACS applied materials & interfaces*, 2018, **10**, 40540-40548.
51. W. Zhao, M. Ding, L. Guo and H. Y. Yang, *Dual-Ion Electrochemical Deionization System with Binder-Free Aerogel Electrodes*, *Small*, 2019, **15**, e1805505.